HHS Public Access

Author manuscript

Nat Mater. Author manuscript; available in PMC 2017 June 26.

Published in final edited form as:

Nat Mater. 2017 April ; 16(4): 489–496. doi:10.1038/nmat4822.

Designer vaccine nanodiscs for personalized cancer immunotherapy

Rui Kuai[1,2], **Lukasz J. Ochyl**[1,2], **Keith S. Bahjat**[3], **Anna Schwendeman**[1,2,§], and **James J. Moon**[1,2,4,§]

[1] Department of Pharmaceutical Sciences, University of Michigan, Ann Arbor, MI 48109, USA

[2] Biointerfaces Institute, University of Michigan, Ann Arbor, MI 48109, USA

[3] Discovery Research, Bristol-Myers Squibb Biologics Discovery California, Redwood City, CA

[4] Department of Biomedical Engineering, University of Michigan, Ann Arbor, MI 48109, USA

Abstract

Despite the tremendous potential of peptide-based cancer vaccines, their efficacy has been limited in humans. Recent innovations in tumor exome sequencing have signaled the new era of personalized immunotherapy with patient-specific neo-antigens, but a general methodology for stimulating strong CD8α+ cytotoxic T-lymphocyte (CTL) responses remains lacking. Here we demonstrate that high density lipoprotein-mimicking nanodiscs coupled with antigen (Ag) peptides and adjuvants can markedly improve Ag/adjuvant co-delivery to lymphoid organs and sustain Ag presentation on dendritic cells. Strikingly, nanodiscs elicited up to 47-fold greater frequencies of neoantigen-specific CTLs than soluble vaccines and even 31-fold greater than perhaps the strongest adjuvant in clinical trials (i.e. CpG in Montanide). Moreover, multi-epitope vaccination generated broad-spectrum T-cell responses that potently inhibited tumor growth. Nanodiscs eliminated established MC-38 and B16F10 tumors when combined with anti-PD-1 and anti-CTLA-4 therapy. These findings represent a new powerful approach for cancer immunotherapy and suggest a general strategy for personalized nanomedicine.

Peptide-based cancer vaccines have been extensively investigated due to their good safety profiles and ease of manufacturing and quality control. However, their anti-tumor efficacy in

§ Co-corresponding authors. J.J.M. (moonjj@umich.edu) or A.S. (annaschw@umich.edu).

Data Availability Statement

All relevant data are available from the authors.

Supplementary Information

Supplementary Information is available in the online version of the paper.

Author contributions

R.K., A.S., and J.J.M. designed the experiments. R.K. performed the experiments. L.J.O. contributed to the tetramer staining assays. R.K., A.S., and J.J.M. analyzed the data and K.S.B. aided in the interpretation of data. R.K. and J.J.M. wrote the paper.

Competing financial interests

A patent application for nanodisc vaccines has been filed (#PCT/US2016/024233, “Compositions and methods for delivery of biomacromolecule agents”) with J.J.M., A.S., and R.K. as inventors, and J.J.M. and A.S. are co-founders of EVOQ Therapeutics, LLC., that develops the nanodisc technology for vaccine applications.

clinical trials has been disappointing, a phenomenon that has been attributed to inefficient co-delivery of Ag peptides and adjuvants to draining lymph nodes (dLNs), and subsequent immunological tolerance and CTL fratricide[1]. Although depot-forming water-in-oil adjuvant systems can improve immunogenicity[2,3], booster immunizations can cause T-cell sequestration at the vaccine site, leading to T-cell exhaustion and deletion[4]. To address these issues, various nano-vaccine systems have been evaluated in animal models with varying degrees of success[5-15]. Despite the progress in the field, potential safety concerns and scale-up manufacturing of nanoparticles, especially in a manner suitable for personalized therapeutics with patient-specific neo-antigens, still remain as the major challenges.

Here we propose an alternative, simple strategy where preformed nanocarriers, with an established clinical manufacturing procedure and excellent safety profiles in humans, are mixed with adjuvants and Ag peptides, including tumor-specific mutant neo-epitopes[16-19], to produce personalized cancer vaccines (**Fig. 1**). Our strategy is based on synthetic high density lipoprotein (sHDL) nanodiscs, composed of phospholipids and apolipoprotein A1 (ApoA1)-mimetic peptides. Compared with other HDLs containing 243-amino acid ApoA1 purified from human plasma or produced recombinantly[20-22], sHDL nanodiscs are synthesized with 22-mer peptides (22A), derived from the repeat α-helix domain of ApoA1[23], with no sequence homology to endogenous ApoA1, thus averting potential trigger of autoimmunity. Importantly, sHDL has been previously manufactured for clinical testing and proven to be safe in humans with the maximum tolerated dose at ~2.2 g/m^2,[24-26] a value one- to two-orders of magnitude greater than most polymeric or inorganic nanoparticles in clinical trials[27,28].

Here we set out to develop a nanodisc-based platform for neo-antigen vaccination (**Fig. 1**). Exploiting the endogenous role of HDL as a nanocarrier for cholesterol, we modified a commonly used oligonucleotide containing 5'-C-phosphate-G-3' (CpG) motif, a potent Toll-like receptor-9 agonist, with cholesterol (Cho-CpG) to enhance its *in vivo* trafficking. We show that preformed sHDL nanodiscs can be simply mixed with cholesteryl-CpG and tumor Ag peptides, including neo-antigens identified via tumor DNA sequencing, to produce homogeneous, stable, and ultrasmall nanodiscs in less than two hours at room temperature (RT). The nanodiscs promote co-delivery of Ag/CpG to dLNs; prolong Ag presentation on antigen-presenting cells (APCs); elicit striking levels of broad-spectrum antitumor T-cell responses that significantly inhibit tumor growth; and eradicate established tumors when combined with immune checkpoint blockade. Based on the facile production process, robust therapeutic efficacy, and clinical safety demonstrated previously[24,25], our approach offers an attractive platform technology for patient-tailored cancer vaccines as well as other bioactive therapeutics.

Engineering nanodiscs for antigen and adjuvant delivery

We first identified lipids and peptides conducive to nanodisc formation. DMPC lipid films were hydrated and added with a series of ApoA1-mimetic peptides, followed by thermal cycling between 50 °C and 4 °C. We identified a subset of peptides, including 22A and D-amino acids of 22A, that produced clear sHDL suspensions, stable for one month when stored at 4°C (**Supplementary Fig. 1a**). In addition, use of phospholipids with transition

temperature (Tm) below RT (e.g. POPC and DOPC with Tm = −2°C and −17°C, respectively) produced murky liposomal suspension, whereas lipids with high Tm (e.g. DPPC and DMPC with Tm = 41°C and 24°C, respectively) formed clear sHDL suspensions in the presence of 22A (**Supplementary Fig. 1b**), showing flexibility in the materials design. Based on their size, homogeneity, and long-term stability, we chose to further investigate 22A and DMPC as the key components of nanodisc vaccines.

To achieve intracellular release of Ag within APCs via reduction-sensitive conjugation of Ag on sHDL, we synthesized dioleoyl-sn-glycero-3-phosphoethanolamine-N-[3-(2-pyridyldithio) propionate] (PDP, **Supplementary Fig. 2**) and incorporated PDP into sHDL (4 mol%). When incubated for 30 min at RT with Ag peptides modified with a cysteine-serine-serine (CSS) linker[29], sHDL nanodiscs were efficiently surface-decorated with various Ag peptides (e.g., $OVA_{257-264}$, a model CD8α+ T-cell epitope Ag from ovalbumin; and Adgpk, neo-antigen in MC-38), and subsequent incubation with Cho-CpG for 30 min at RT led to almost complete (~98%) insertion of CpG into sHDL, producing nanodiscs co-loaded with Ag and CpG (termed sHDL-Ag/CpG, with ~6.5 Ag peptides and ~1 CpG molecule per nanodisc, **Supplementary Fig. 3, Supplementary Table 1**). sHDL-Ag/CpG exhibited uniform disc-like morphology with an average diameter of 10.5 ± 0.5 nm and polydispersity index of 0.20 ± 0.02 (**Fig. 2a,b**). Importantly, sHDL-Ag/CpG could be readily sterile-filtered and stored frozen at −20 °C for at least 8 weeks before thawing at 37 °C, without negatively affecting its homogeneity (**Fig. 2c**).

Sustained antigen presentation and cross-priming of T-cells

We next examined the impact of nanodiscs on Ag presentation. Bone marrow derived dendritic cells (BMDCs) pulsed for 24 h with sHDL-CSSSIINFEKL/CpG presented $OVA_{257-264}$ SIINFEKL with a greater efficiency than BMDCs treated with free Ag peptides admixed with CpG or sHDL-CSSSIINFEKL, as determined by staining DCs with the 25-D1.16 mAb directed against SIINFEKL-H-$2K^b$ complexes (**Fig. 2d, Supplementary Fig. 4a,b**). Interestingly, DCs pulsed with free SIINFEKL+CpG efficiently presented Ag for the first 6 h of incubation, but Ag presentation decreased precipitously past 6 h (**Fig. 2e,f, Supplementary Fig. 4c**), suggesting initial direct Ag binding to MHC-I molecules, followed by rapid Ag degradation or disassociation. In contrast, Ag presentation with sHDL-Ag/CpG gradually increased over time, achieving ~9-fold greater levels at 24 h and maintaining ~4-fold higher levels even at 48 h, compared with free SIINFEKL+CpG.

Intrigued by prolonged Ag presentation, we investigated the process of nanodisc uptake and Ag localization using CSS-$SIINFEK_{(FITC)}L$; SIINFEKL modified with FITC at ε-amino group in the lysine residue is known to retain its binding capacity to H-$2K^b$ molecules[30]. JAWSII cells (immortalized immature DCs) incubated with free Ag(FITC)+CpG displayed weak fluorescence signal on the plasma membrane at 6 h, and only dim fluorescence was observed by 24 h (**Fig. 2g, Supplementary Fig. 5**). In stark contrast, sHDL-Ag(FITC)/CpG treatment led to strong FITC signal co-localized with endosomes/lysosomes by 6 h, and robust Ag(FITC) signal was detected on cell membranes by 24 h and sustained up to 48 h. In addition, nanodiscs containing Rh-PE or Texas Red-labeled-22A were predominantly found within endosomes/lysosomes, indicating cellular uptake of intact whole nanodiscs

(**Supplementary Fig. 6**). To assess the impact of prolonged Ag presentation on T-cell cross-priming, we treated BMDCs with free Ag peptides+CpG or sHDL-Ag/CpG for 24 or 48 h, and then added SIINFEKL-specific, H-2K^b-restricted B3Z T-cell hybridomas. BMDCs pulsed with sHDL-Ag/CpG promoted strong B3Z T-cell activation even after 48 h incubation, whereas free Ag peptides+CpG induced minimal B3Z T-cell activation beyond the 24 h period (**Fig. 2h**). Moreover, sHDL-Ag/CpG potently stimulated DC maturation (**Supplementary Fig. 7**). Altogether, whereas free Ag peptide was rapidly loaded and dissociated from MHC-I molecules on cell membranes, nanodiscs facilitated intracellular delivery of Ag/CpG and mediated their sustained release within endosomes/lysosomes, thereby promoting durable Ag presentation, APC maturation, and cross-priming CD8α+ T-cells *in vitro*.

Elicitation of robust, long-lived T-cells responses *in vivo*

We next investigated the impact of nanodiscs on lymphatic delivery of Ag/CpG and induction of CD8α+ T-cell responses *in vivo*[5]. C57BL/6 mice injected subcutaneously at tail base with 31 nmol free CSS-SIINFEK$_{(FITC)}$L had minimal FITC signal in inguinal dLNs after 1 day (**Fig. 3a**), potentially due to systemic dissemination of small MW Ag peptide or direct Ag binding on non-APCs at the injection site[1]. In contrast, sHDL-Ag group exhibited markedly increased FITC signal in dLNs ($p < 0.01$, **Fig. 3a**), with Ag(FITC) and Cy5-tagged 22A co-localized within dLNs (**Supplementary Fig. 8**). Similarly, injection of 2.3 nmol Cy5-tagged Cho-CpG in sHDL increased its LN accumulation, compared with injection in free soluble form ($p < 0.01$, **Fig. 3b**). These results showed that sHDL nanodisc promoted co-delivery of Ag and CpG to dLNs. We next immunized C57BL/6 mice with 15.5 nmol Ag and 2.3 nmol CpG (non-fluorophore tagged), and peripheral blood was analyzed for the frequency of SIINFEKL–MHC-I tetramer+ CD8α+ T-cells. The mixture of free Ag peptides (SIINFEKL or CSS-SIINFEKL) and CpG induced 1-3% Ag-specific CTLs after the third immunization (**Fig. 3c,d**). As the benchmark, we also vaccinated animals with the equivalent doses of Ag and CpG emulsified in water-in-oil Montanide, which is arguably one of the strongest adjuvant systems in clinical trials for peptide-based cancer vaccines[2,3,31,32]. Ag +CpG+Montanide elicited ~2% Ag-specific CTLs after priming; however, no further T-cell expansion was observed even after the third immunization, consistent with a recent study reporting dysfunction and deletion of high-avidity T-cells after repeated immunizations with a depot-forming water-in-oil adjuvant[4]. In contrast, sHDL-Ag/CpG group elicited a peak frequency of ~21% Ag-specific CD8α+ T-cells after the third vaccination ($p < 0.0001$, **Fig. 3c,d**). We observed similar levels of peak Ag-specific CTL responses after sHDL-Ag/CpG vaccination with the dosing intervals of 1, 2, or 3 weeks (**Supplementary Fig. 9**). When challenged with 2×10^5 B16OVA cells, mice immunized with sHDL-Ag/CpG had no detectable tumor masses up to 28 days, whereas mice immunized with free Ag peptides +CpG or Ag+CpG+Montanide all succumbed to tumors with marginal survival benefits (**Fig. 3e, Supplementary Fig. 10**). Importantly, throughout our studies, we did not observe any signs of toxicity, autoimmunity, nor immune responses directed against the ApoA1-mimetic peptide 22A in animals immunized multiple times with sHDL-Ag/CpG (**Supplementary Fig. 11**).

We sought to rule out the possibility that CSS-modified peptides or Cho-CpG dissociated from sHDL-Ag/CpG *in vivo* were responsible for the strong CTL responses. Introducing the CSS linker to SIINFEKL and replacing free CpG with Cho-CpG in free soluble form resulted in minimal T-cell responses, and the physical mixture of Ag, CpG, and sHDL also elicited weak CTL responses (**Fig. 3f**). In contrast, sHDL-Ag/CpG nanodiscs drastically improved CD8α+ T-cell responses, eliciting remarkable 41-fold greater frequency of Ag-specific CD8α+ T-cells than CSSSINFEKL+Cho-CpG group (day 35, $p < 0.0001$), with CTLs primarily exhibiting $CD44^{high}CD62L^{low}$ effector phenotype and robust IFN-γ^+ ELISPOT responses (**Fig. 3f,g, Supplementary Fig. 12**). We also examined the durability of T-cell responses; after achieving their peak ~30% responses, animals still maintained 10% Ag-specific CD8α+ T-cells at 2 months post the last vaccination (20-fold greater than free Ag+CpG group, $p < 0.001$, **Fig. 3h**), and efficiently eliminated B16OVA cells inoculated intravenously (**Fig. 3i**), demonstrating long-lived protection against tumor challenge. In contrast, the soluble vaccine failed to protect animals against the intravenous B16OVA challenge.

Tumor regression by combination neo-antigen immunotherapy

To demonstrate the utility of our platform technology for vaccination against neo-antigens, we first employed the murine MC-38 colon carcinoma model recently reported to harbor a single-epitope mutation within Adpgk protein (ASMTN**R**ELM → ASMTN**M**ELM), with the neo-epitope presented in MHC-I H-$2D^b$ molecules[16]. We confirmed the Adpgk neo-antigen mutation in MC-38 cells by cDNA sequencing (**Fig. 4a, Supplementary Fig. 13**) and synthesized sHDL-Adpgk/CpG by mixing nanodiscs with the neo-epitope modified with the CSS-linker and Cho-CpG. C57BL/6 mice immunized with sHDL-Adpgk/CpG generated remarkable 47-fold and 31-fold greater frequencies of neoantigen-specific CTLs, compared with the soluble Adpgk+CpG and Adpgk+CpG+Montanide groups, respectively ($p < 0.0001$, **Fig. 4b,c**), with tumor-specific cytotoxicity against MC-38 target cells (**Supplementary Fig. 14**) and long-lived T-cell responses, as in the case of sHDL-SIINFEKL/CpG vaccination (**Fig. 4d**). To investigate the therapeutic efficacy of nanodisc vaccination, C57BL/6 mice were inoculated subcutaneously with 10^5 MC-38 cells and treated with 15.5 nmol Adpgk and 2.3 nmol CpG (**Fig. 4e**). Therapeutic vaccination with sHDL-Adpgk/CpG induced polyfunctional IFN-γ^+ and IFN-γ^+TNF-α^+ Adpgk-specific CD8α+ T-cells and substantially slowed MC-38 tumor growth (**Fig. 4e**), compared with the traditional soluble Adpgk+CpG vaccine. However, no tumor rejection was observed in either vaccine groups, potentially due to immunosuppression within tumor microenvironment, as we detected high expression levels of programmed cell death-1 (PD-1) and its ligand PD-L1 among tumor-infiltrating CD8α+ T-cells and tumor cells, respectively (**Supplementary Fig. 15**). In order to block the immunosuppressive PD-1/PD-L1 pathway[33,34], we combined the vaccines with anti-PD-1 antibodies (αPD-1). Combination immunotherapy with sHDL-Adpgk/CpG and αPD-1 treatment generated robust neoantigen-specific CTL responses and led to complete tumor regression in ~88% mice (**Fig. 4f, Supplementary Fig. 16)**, compared with ~25% rate of tumor regression in the soluble Adpgk+CpG+αPD-1 group. Notably, 100% of surviving mice rejected the subsequent re-challenge with MC-38 cells

inoculated at the contralateral flank on day 70, indicating immunological memory against tumor recurrence (data not shown).

Multi-epitope T-cell responses with cocktail nanodiscs

Finally, we evaluated our nanodisc platform in a melanoma model with B16F10 cells, as they are highly aggressive, poorly immunogenic, and hence hard to treat with conventional cancer vaccines. To prevent tumor immune escape by loss of a single mutant allele[35], we sought to elicit broad-spectrum T-cell responses by employing multiple antigens (multiAgs), including recently reported B16F10 mutated neo-epitopes (MHC I-restricted M27 and MHC II-restricted M30) as well as MHC I-restricted epitope from tyrosinase-related protein 2 (TRP2, a melanoma-associated Ag), all loaded in the same nanodiscs. C57BL/6 mice inoculated subcutaneously with 10^5 B16F10 cells were vaccinated with sHDL-multiAgs/CpG, eliciting a total of ~30% Ag-specific, IFN-γ^+ CD8α+ and CD4+ T-cells in peripheral blood, compared with only 1-3% induced by the soluble multiAgs+CpG or multiAgs+CpG +Montanide groups ($p < 0.0001$, **Fig. 5a, Supplementary Fig. 17)**. Vaccination with sHDL-multiAgs/CpG significantly inhibited B16F10 tumor growth, compared with the soluble or Montanide vaccines ($p < 0.0001$, **Fig. 5b**). Notably, removing either M27/M30 or TRP2 from sHDL-multiAgs/CpG compromised its therapeutic efficacy, suggesting the benefits of broad CTL responses against neo-antigens and tumor-associated antigens (**Fig. 5c**). Lastly, we evaluated sHDL-multiAgs/CpG combined with dual immune checkpoint inhibitors. Combination immunotherapy with sHDL-multiAgs/CpG and αPD-1/αCTLA-4 treatment led to an impressive rate of B16F10 tumor rejection with ~90% of mice free of tumor, whereas the soluble multiAgs+CpG+αPD-1/αCTLA-4 treatment mediated tumor regression in ~38% of animals (**Fig. 5d**).

Overall, our results have significant clinical importance since these nanodiscs, with an established manufacturing procedure suited for neo-antigen vaccination and excellent safety profiles in humans, can drastically improve co-delivery of antigens and adjuvants to LNs (**Fig. 3a,b**); sustain antigen presentation on DCs and cross-priming of T-cells (**Fig. 2e-h**); drive multivalent CD8α+ and CD4+ T-cell immunity against neo-antigens and tumor-associated antigens (**Fig. 3c-g, Fig. 4b-e, Fig. 5a**) with long-term T-cell response (**Fig. 3h,i**); and significantly delay tumor growth in the setting of therapeutic vaccination (**Fig. 4e, Fig. 5b,c**). However, despite strong anti-tumor T-cell responses, nanodiscs administered as a monotherapy failed to eliminate tumors, possibly due to the immunosuppressive PD-L1/PD-1 pathway within the tumor microenvironment (**Supplementary Fig. 15**). Aiming to unleash the full cytotoxic potential of T-cells[33,34], we combined nanodisc vaccination with immune checkpoint inhibitors, achieving potently amplified therapeutic efficacy and eradication of MC-38 and B16F10 tumors in > 85% of animals (**Fig. 4f, Fig. 5d**). Although other nanosystems in the literature[5-15] may be also applicable, this is, to the best of our knowledge, the first demonstration of antitumor efficacy with personalized nanomedicine tailored with tumor-specific neo-antigens.

While the work presented here provides the framework for future clinical translation, our strategy designed to generate neoantigen-specific cellular immunity requires tumor DNA/RNA exome sequencing, identification of neo-antigens, and production of nanodiscs,

followed by a multi-dose vaccine regimen, which collectively may protract the time window required for control of malignancies for late-stage patients. These issues may be tackled in the future by multi-thronged strategies that exploit combined immunotherapy targeted to humoral and innate arms of immunity[36] or radiation therapy[37] and select chemotherapeutics[38] known to delay tumor growth and synergize with T-cell vaccines.

In conclusion, we have developed a new nano-vaccine system ideally suited for individualized neo-epitope vaccination and demonstrated their potency to generate broad-spectrum T-cell responses with striking therapeutic efficacy when combined with immune checkpoint inhibitors. As the majority of somatic mutations in cancer cells are unique to each patient, cancer vaccines would require a personalized approach[16-19]. Coupled with the recent biomedical breakthroughs in neo-antigen screening and immune checkpoint blockade[33,34,39-41], our approach may offer a powerful yet facile strategy for producing cancer vaccines designed for each patient. Furthermore, this platform technology may be generally applicable for personalized therapeutics with a wide range of bioactive molecules and imaging agents.

METHODS

Synthesis and characterization of sHDL nanodiscs

Dioleoyl-*sn*-glycero-3-phosphoethanolamine-N-[3-(2-pyridyldithio) propionate] (DOPE-PDP) was synthesized as reported previously[42]. DMPC and DOPE-PDP (molar ratio = 96:4) were dissolved in chloroform. The mixture was dried with nitrogen flow and placed under vacuum for at least 1 h. The resulting lipid film was hydrated in 10 mM sodium phosphate buffer and sonicated in a bath sonicator for 10 min, followed by probe sonication for another 2.5 min. ApoA1 mimetic peptide 22A dissolved in endotoxin free water was added to the above mixture (22A:lipids = 1:7.5 molar ratio), which was then subjected to three heating and cooling cycles to obtain sHDL. To conjugate tumor antigen peptides to sHDL, cysteine terminated tumor antigen peptides were added to the above sHDL (antigen peptide:DOPE-PDP = 2.5:1, molar ratio) and incubated at room temperature with gentle shaking on an orbital shaker. To construct sHDL nanodiscs with multi-antigens, each antigen peptide was reacted with DOPE-PDP (antigen peptide:DOPE-PDP = 1.5:1, molar ratio) for 1 h in dimethylformamide (DMF), which was removed by freeze-drying after dilution with endotoxin-free water. The lipid-peptide conjugates were added to pre-formed sHDL and incubated for 30 min at room temperature. Unreacted tumor antigen peptides were removed by using Zeba Spin Desalting columns (Pierce). Antigen peptides used in our studies include $OVA_{257\text{-}264}$ SIINFEKL, CSSSIINFEKL, CSSSIINFEK(FITC)L, $TRP2_{180\text{-}188}$ SVYDFFVWL, CSVYDFFVWL, M27 neo-epitope LCPGNKYEM, M30 neo-epitope CSSVDWENVSPELNSTDQ, *Adpgk* mutant peptide ASMTNMELM (all obtained from GenScript Corp., Piscataway, NJ), and CSSASMENMELM (from AnaSpec, Fremont, CA). The conjugation efficiency of tumor antigen peptides was calculated based on the decrease of absorbance signal associated with DOPE-PDP as determined by HPLC. The loading efficiency of tumor antigen peptides in sHDL was confirmed by using FITC-labeled peptides and measuring the fluorescence intensity of sHDL formulations at Ex = 490 nm and Em = 520 nm after dissolving the formulations in PBS containing 1% Triton X-100. To load CpG

in sHDL, different concentrations (0-200 μg/mL) of cholesterol modified CpG 1826 (Cho-CpG, Integrated DNA Technologies, Coralville, IA) were incubated with sHDL at room temperature with gentle shaking on an orbital shaker. The amount of CpG incorporated into sHDL and free CpG was analyzed by gel permeation chromatography (GPC) equipped with TSKgel G2000SWxl column (7.8 mm ID × 30 cm, Tosoh Bioscience LLC). The sHDL formulations were diluted to 0.5 mg/mL 22A with PBS, and the particle sizes were measured by dynamic light scattering (DLS, Zetasizer Nano ZSP, Malvern, UK). The morphology of sHDL was observed by transmission electron microscopy (TEM) after proper dilution of the original samples with 1% uranyl acetate solution negative staining. All images were acquired on JEM 1200EX electron microscope (JEOL USA, Peabody, MA) equipped with an AMT XR-60 digital camera (Advanced Microscopy Techniques Corp. Woburn, MA).

BMDC activation, antigen presentation, and cross-priming

BMDCs were prepared as described previously[43]. Immature BMDCs were plated at 1×10^6 cells/well in 12-well plates. After 24 h, BMDCs were incubated with 75 nM CpG and/or 500 nM antigen peptide in various formulations or 0.5 μg/mL LPS (positive control) in complete media for different lengths of time (2, 6, 24, and 48 h) at 37 °C with 5% CO_2. BMDCs were harvested, washed with FACS buffer (1% BSA in PBS), incubated with anti-CD16/32 at room temperature, and then stained on ice with fluorophore-labeled antibodies against CD11c, CD40, CD80, and CD86, or PE-conjugated anti-mouse SIINFEKL/H-2K^b mAb 25-D1.16 (eBioscience, San Diego, CA). Cells were then washed twice by FACS buffer, resuspended in 2 μg/ml DAPI solution, and analyzed by flow cytometry (Cyan 5, Beckman Coulter, USA). To assess cross-priming of T-cells, BMDCs were incubated with different formulations of SIINFEKL (20, 100 and 500 nM) and CpG (3, 15, and 75 nM) for 24 h or 48 h at 37 °C. Cells were then carefully washed 3 times with PBS, and 10^5 B3Z CD8+ T hybridoma cells (kindly provided by Dr. N. Shastri) per well were added in RPMI 1640 supplemented with 10% FBS, 2 mM L-glutamine, 55 μM β-mercaptoethanol, 1 mM pyruvate, 100 U/mL penicillin and 100 μg/mL streptomycin. Throughout the studies, all cells were used as received and tested negative for mycoplasma contamination and rodent pathogens. After 24 hr of incubation, the media were aspirated, and 150 μL CPRG/lysis buffer (0.15 mM chlorophenol red- β-D-galactopyranoside (CPRG), 0.1% Triton-X 100, 9 mM MgCl2, 100 μM mercaptoethanol in PBS) was added. The plates were incubated at 37 °C in the dark for 90 min, after which the absorbance of released chlorophenol red was measured at 570 nm using a microplate reader. To visualize intracellular distribution of nanodiscs, JAWSII cells (ATCC, Manassas, VA) were seeded at 1×10^6 cells on 35 mm petri dishes (MatTek Corp., Ashland, MA) and incubated with the physical mixture of free CSSSIINFEK(FITC)L and CpG, or sHDL-CSSSIINFEK(FITC)L/CpG for different lengths of time (6, 24, and 48 h). Cells were then washed 3 times with PBS and incubated for 30 min at 37 °C with 50 nM LysoTracker® Red DND-99 (Invitrogen) and 2 μg/mL Hoechst in phenol/serum-free media to stain lysosomes and nuclei, respectively. In some studies, the lipid layers of sHDL were incorporated with 0.5 mol % DOPE-Rhod and 22A peptide of sHDL was labeled by incubating pre-formed sHDL with Texas Red®-X succinimidyl ester (Life Technologies). JAWSII cells were then imaged using a confocal microscope (Nikon A1).

In vivo immunization and cancer immunotherapy studies

Animals were cared for following federal, state, and local guidelines. All work performed on animals was in accordance with and approved by University Committee on Use and Care of Animals (UCUCA) at University of Michigan, Ann Arbor. Female C57BL/6 mice of age 6–8 weeks (Harlan Laboratories) were immunized with different formulations containing antigen peptides (15.5 nmol/mouse) and CpG (2.3 nmol/mouse) in 100 μl volume by subcutaneous injection at the tail base on indicated time points. In some studies, antigen peptide and CpG emulsified in Montanide served as a positive control. Briefly, antigen peptide (155 nmol) and CpG (23 nmol) in 0.5 mL PBS were thoroughly emulsified in 0.5 mL Montanide until the mixture was homogeneous and administered subcutaneously in 100 μl injection volume. For lymph node draining studies, C57BL/6 mice were injected with free CSSSIINFEK(FITC)L, sHDL-CSSSIINFEK(FITC)L, free Cho-CpG(Cy5), or sHDL-Cho-CpG(Cy5). After 24 h, inguinal lymph nodes were harvested, and FITC or Cy5 fluorescence signal was measured with IVIS optical imaging system (Caliper Life Sciences). In some studies, induction of IgG response against 22A peptide was assessed by ELISA on immune sera as described previously[44]. The highest dilution with twice the absorbance of background was considered as the end-point dilution titer.

For prophylactic tumor challenge studies, vaccinated animals were challenged on day 8 after last immunization by subcutaneous injection of 2×10^5 B16OVA cells (kindly provided by Dr. Kenneth Rock) per mouse on the right flank. Tumor growth was monitored every other day, and the tumor volume throughout this study was calculated by the following equation[45]: tumor volume = length × width^2 × 0.52. Animals were euthanized when the tumor masses reached 1.5 cm in diameter or when animals became moribund with severe weight loss or ulceration. For the lung metastasis model, vaccinated animals were challenged by intravenous injection of 5×10^4 B16OVA cells/mouse, and lungs excised on day 20 were stained in Fekete's solution, followed by enumeration of B16OVA lung tumor nodules. For therapeutic tumor vaccination studies, C57BL/6 mice were inoculated with 1×10^5 MC38 (kindly provided by Dr. Weiping Zou) or B16F10 cells (ATCC) per mouse on the right flank by subcutaneous injection on day 0 and vaccinated on indicated days. For the combinatorial immunotherapy, anti-mouse PD-1 (100 μg/mouse, clone:RMP1-14, BioXcell, West Lebanon, NH) and/or anti-mouse CTLA-4 (100 μg/mouse, clone:9D9, BioXcell) antibodies were administered intraperitoneally on days 1 and 4 after each vaccination. Tumor growth was monitored as indicated above.

Phenotypic and functional assessment of T-cells

Immunized mice were analyzed for the percentages of tumor antigen-specific CD8α+ T cells using the tetramer staining assay as described previously[46,47] with peptide-MHC tetramer tagged with PE (e.g. H-2K^b-restricted SIINFEKL (Beckman Coulter) or H-2D^b-restricted ASMTNMELM (the NIH Tetramer Core Facility, Atlanta, GA)). CTL cytotoxicity was evaluated using the Lactate Dehydrogenase (LDH) Assay (CytoTox 96® Non-Radioactive Cytotoxicity Assay) in vitro with splenocytes from immunized mice and MC-38 target cells, as described previously[48,49]. ELISPOT assay was performed with splenocytes from immunized mice as described previously[50]. The intracellular cytokine staining (ICS) assays on PBMCs were performed with anti-IFN-γ-PE and anti-TNF-α-FITC as described

previously[6]. For analysis of tumor-infiltrating T-cells, tumor tissues were excised at indicated time points, cut into small pieces of 2-4 mm, and then placed in dissociation buffer (1 mg/mL of collagenase type IV and 0.1 mg/mL of DNase I in RPMI) for 30 min at 37 °C with gentle shaking. The cell suspension was passed through a 70-μm strainer, washed with FACS buffer, stained with indicated antibodies, followed by flow cytometric analysis.

cDNA sequencing of neo-epitope (Adpgk) in MC-38 cells

Total RNA was extracted from MC-38 cells by the RNeasy® mini Kit (QIAGEN) following the manufacturer's instructions. The first-strand cDNA was synthesized using 1 μg of total RNA with the SuperScript™ III First-Strand Synthesis SuperMix Kit (Invitrogen). Adpgk cDNA with lengths of 250 bp and 485 bp were selectively amplified by using the following two sets of sequence specific primers. Primer 1: TGCCAACCGCTTCATCTTCT (forward primer) and GGTAGACCAGCGTGTGGAAA (reverse primer); Primer 2: CTCCAACGGGGCCATGAATA (forward primer) and CGTGGGAAAGACCTGCTGAT (reverse primer). The amplification was performed using the SuperScript One Step RT-PCR System (Invitrogen). The final cDNA products were visualized in 1.5% agarose gels with ethidium bromide, and the Adpgk cDNA bands were cut and purified using the PureLink® Quick Gel Extraction and PCR Purification Combo Kit (Invitrogen). The purified cDNA was sequenced by the Sanger sequencing method at the University of Michigan DNA Sequencing Core.

Statistical analysis

Sample sizes were chosen based on preliminary data from pilot experiments and previously published results in the literature. All animal studies were performed after randomization. Experiments were not performed in a blinded fashion. Data were analyzed by one- or two-way analysis of variance (ANOVA), followed by Bonferroni *post hoc* test for comparison of multiple groups with Prism 5.0 (GraphPad Software). Data were normally distributed and variance between groups was similar. P values less than 0.05 were considered statistically significant. All values are reported as means ± SD with the indicated sample size. No samples were excluded from analysis.

Supplementary Material

Refer to Web version on PubMed Central for supplementary material.

Acknowledgements

This work was supported in part by NIH (R01GM113832, A.S.; R21NS091555, A.S.; UL1TR000433, J.J.M.; 1K22AI097291, J.J.M.; R01EB022563, J.J.M.; R01AI127070, J.J.M.), AHA (13SDG17230049, A.S.), UM MTRAC for Life Sciences (A.S.), and the UM College of Pharmacy faculty start-up fund (J.J.M., A.S.). J.J.M. is a Young Investigator supported by the Melanoma Research Alliance (348774), DoD/CDMRP Peer Reviewed Cancer Research Program (W81XWH-16-1-0369), and NSF CAREER Award (1553831). R.K. is supported by the Broomfield International Student Fellowship and the AHA Pre-doctoral Fellowship (15PRE25090050). L.O. is supported by pre-doctoral fellowships from UM Rackham and AFPE. We acknowledge Joel Whitfield for his technical assistance with ELISPOT and thank Robert H. Lyons, Luis Villa Diaz, Jin Koo Kim, and Prof. Paul H. Krebsbach for their contributions to cDNA sequencing. We acknowledge Prof. Darrell J. Irvine (MIT) and Prof. Nicholas A. Kotov (UM) for critical review of the manuscript; the University of Michigan Consulting for Statistics, Computing, and Analytics Research (CSCAR) for help with statistical analyses; the NIH Tetramer Core Facility (contract HHSN272201300006C) for provision of MHC-I tetramers; Dr. N. Shastri (University of California, Berkeley) for B3Z T cell hybridoma; Dr. Kenneth Rock (University of Massachusetts, Amherst, MA) for B16OVA

cells; and Dr. Weiping Zou (University of Michigan, Ann Arbor, MI) for MC-38 cells. Opinions interpretations, conclusions and recommendations are those of the author and are not necessarily endorsed by the Department of Defense.

REFERENCES

1. Melief CJ, van der Burg SH. Immunotherapy of established (pre)malignant disease by synthetic long peptide vaccines. Nat Rev Cancer. 2008; 8:351–360. [PubMed: 18418403]
2. Speiser DE, et al. Rapid and strong human CD8+ T cell responses to vaccination with peptide, IFA, and CpG oligodeoxynucleotide 7909. J Clin Invest. 2005; 115:739–746. [PubMed: 15696196]
3. Fourcade J, et al. Immunization with analog peptide in combination with CpG and montanide expands tumor antigen-specific CD8+ T cells in melanoma patients. J Immunother. 2008; 31:781–791. [PubMed: 18779741]
4. Hailemichael Y, et al. Persistent antigen at vaccination sites induces tumor-specific CD8+ T cell sequestration, dysfunction and deletion. Nat Med. 2013; 19:465–472. [PubMed: 23455713]
5. Reddy ST, et al. Exploiting lymphatic transport and complement activation in nanoparticle vaccines. Nat Biotechnol. 2007; 25:1159–1164. [PubMed: 17873867]
6. Moon JJ, et al. Interbilayer-crosslinked multilamellar vesicles as synthetic vaccines for potent humoral and cellular immune responses. Nat Mater. 2011; 10:243–251. [PubMed: 21336265]
7. Lee IH, et al. Imageable antigen-presenting gold nanoparticle vaccines for effective cancer immunotherapy in vivo. Angew Chem Int Ed Engl. 2012; 51:8800–8805. [PubMed: 22847719]
8. Li AV, et al. Generation of effector memory T cell-based mucosal and systemic immunity with pulmonary nanoparticle vaccination. Sci Transl Med. 2013; 5:204ra130.
9. Jeanbart L, et al. Enhancing efficacy of anticancer vaccines by targeted delivery to tumor- draining lymph nodes. Cancer Immunol Res. 2014; 2:436–447. [PubMed: 24795356]
10. Xu Z, Wang Y, Zhang L, Huang L. Nanoparticle-delivered transforming growth factor- beta siRNA enhances vaccination against advanced melanoma by modifying tumor microenvironment. ACS Nano. 2014; 8:3636–3645. [PubMed: 24580381]
11. Liu H, et al. Structure-based programming of lymph-node targeting in molecular vaccines. Nature. 2014; 507:519–522. [PubMed: 24531764]
12. Rosalia RA, et al. CD40-targeted dendritic cell delivery of PLGA-nanoparticle vaccines induce potent anti-tumor responses. Biomaterials. 2015; 40:88–97. [PubMed: 25465442]
13. Chiu YC, Gammon JM, Andorko JI, Tostanoski LH, Jewell CM. Modular vaccine design using carrier-free capsules assembled from polyionic immune signals. ACS Biomater Sci Eng. 2015; 1:1200–1205. [PubMed: 26689147]
14. Fan Y, Moon JJ. Nanoparticle Drug Delivery Systems Designed to Improve Cancer Vaccines and Immunotherapy. Vaccines (Basel). 2015; 3:662–685. [PubMed: 26350600]
15. Lizotte PH, et al. In situ vaccination with cowpea mosaic virus nanoparticles suppresses metastatic cancer. Nat Nanotechnol. 2016; 13:295–303.
16. Yadav M, et al. Predicting immunogenic tumour mutations by combining mass spectrometry and exome sequencing. Nature. 2014; 515:572–576. [PubMed: 25428506]
17. Kreiter S, et al. Mutant MHC class II epitopes drive therapeutic immune responses to cancer. Nature. 2015; 520:692–696. [PubMed: 25901682]
18. Rajasagi M, et al. Systematic identification of personal tumor-specific neoantigens in chronic lymphocytic leukemia. Blood. 2014; 124:453–462. [PubMed: 24891321]
19. Schumacher TN, Schreiber RD. Neoantigens in cancer immunotherapy. Science. 2015; 348:69–74. [PubMed: 25838375]
20. Wolfrum C, et al. Mechanisms and Optimization of *in Vivo* Delivery of Lipophilic siRNAs. Nat Biotechnol. 2007; 25:1149–1157. [PubMed: 17873866]
21. Fischer NO, et al. Colocalized delivery of adjuvant and antigen using nanolipoprotein particles enhances the immune response to recombinant antigens. J Am Chem Soc. 2013; 135:2044–2047. [PubMed: 23331082]
22. Duivenvoorden R, et al. A statin-loaded reconstituted high-density lipoprotein nanoparticle inhibits atherosclerotic plaque inflammation. Nat Commun. 2014; 5:3065. [PubMed: 24445279]

23. Li, D., Gordon, S., Schwendeman, A., Remaley, AT. Apolipoprotein Mimetics in the Management of Human Disease. Springer; Switzerland: 2015. Apolipoprotein mimetic peptides for stimulating cholesterol efflux; p. 29-42.
24. Khan M, Lalwani N, Drake S, Crockatt J, Dasseux J. Single-dose intravenous infusion of ETC-642, a 22-Mer ApoA-I analogue and phospholipids complex, elevates HDL- C in atherosclerosis patients. Circulation. 2003; 108(Suppl IV):563–564.
25. Miles J, et al. Single-dose tolerability, pharmacokinetics, and cholesterol mobilization in HDL-C fraction following intravenous administration of ETC-642, a 22-mer ApoA-I analogue and phospholipids complex, in atherosclerosis patients. Proceedings of Arterioscler Thromb Vasc Biol. 2004; 24:E19.
26. Kuai R, Li D, Chen YE, Moon JJ, Schwendeman A. High-Density Lipoproteins: Nature's Multifunctional Nanoparticles. ACS Nano. 2016; 10:3015–3041. [PubMed: 26889958]
27. Alexis F, Pridgen E, Molnar LK, Farokhzad OC. Factors affecting the clearance and biodistribution of polymeric nanoparticles. Mol Pharm. 2008; 5:505–515. [PubMed: 18672949]
28. Anselmo AC, Mitragotri S. A Review of Clinical Translation of Inorganic Nanoparticles. AAPS J. 2015; 17:1041–1054. [PubMed: 25956384]
29. Hirosue S, Kourtis IC, van der Vlies AJ, Hubbell JA, Swartz MA. Antigen delivery to dendritic cells by poly(propylene sulfide) nanoparticles with disulfide conjugated peptides: Cross-presentation and T cell activation. Vaccine. 2010; 28:7897–7906. [PubMed: 20934457]
30. Saini SK, et al. Dipeptides promote folding and peptide binding of MHC class I molecules. Proc Natl Acad Sci U S A. 2013; 110:15383–15388. [PubMed: 24003162]
31. US National Library of Medicine. ClinicalTrials.gov [online]. 2016. http://clinicaltrials.gov/show/NCT00819806
32. US National Library of Medicine. ClinicalTrials.gov [online]. 2016. http://clinicaltrials.gov/ct2/show/record/NCT00640861
33. Topalian SL, et al. Safety, activity, and immune correlates of anti-PD-1 antibody in cancer. N Engl J Med. 2012; 366:2443–2454. [PubMed: 22658127]
34. Zou W, Wolchok JD, Chen L. PD-L1 (B7-H1) and PD-1 pathway blockade for cancer therapy: Mechanisms, response biomarkers, and combinations. Sci Transl Med. 2016; 8:328rv324.
35. Verdegaal EM, et al. Neoantigen landscape dynamics during human melanoma-T cell interactions. Nature. 2016; 536:91–5. [PubMed: 27350335]
36. Moynihan KD, et al. Eradication of large established tumors in mice by combination immunotherapy that engages innate and adaptive immune responses. Nat Med. 2016
37. Formenti SC, Demaria S. Combining radiotherapy and cancer immunotherapy: a paradigm shift. J Natl Cancer Inst. 2013; 105:256–265. [PubMed: 23291374]
38. Kang TH, et al. Chemotherapy acts as an adjuvant to convert the tumor microenvironment into a highly permissive state for vaccination-induced antitumor immunity. Cancer Res. 2013; 73:2493–2504. [PubMed: 23418322]
39. Gubin MM, et al. Checkpoint blockade cancer immunotherapy targets tumour-specific mutant antigens. Nature. 2014; 515:577–581. [PubMed: 25428507]
40. Robbins PF, et al. Mining exomic sequencing data to identify mutated antigens recognized by adoptively transferred tumor-reactive T cells. Nat Med. 2013; 19:747–752. [PubMed: 23644516]
41. Linnemann C, et al. High-throughput epitope discovery reveals frequent recognition of neo-antigens by CD4+ T cells in human melanoma. Nat Med. 2015; 21:81–85. [PubMed: 25531942]
42. Kuai R, et al. Efficient delivery of payload into tumor cells in a controlled manner by TAT and thiolytic cleavable PEG co-modified liposomes. Mol Pharm. 2010; 7:1816–1826. [PubMed: 20701288]
43. Lutz MB, et al. An advanced culture method for generating large quantities of highly pure dendritic cells from mouse bone marrow. J Immunol Methods. 1999; 223:77–92. [PubMed: 10037236]
44. DeMuth PC, Moon JJ, Suh H, Hammond PT, Irvine DJ. Releasable layer-by- layer assembly of stabilized lipid nanocapsules on microneedles for enhanced transcutaneous vaccine delivery. ACS Nano. 2012; 6:8041–8051. [PubMed: 22920601]

45. Gorrin-Rivas MJ, et al. Mouse macrophage metalloelastase gene transfer into a murine melanoma suppresses primary tumor growth by halting angiogenesis. Clin Cancer Res. 2000; 6:1647–1654. [PubMed: 10815882]

46. Ochyl LJ, Moon JJ. Whole-animal imaging and flow cytometric techniques for analysis of antigen-specific CD8+ T cell responses after nanoparticle vaccination. J Vis Exp. 2015:e52771. [PubMed: 25992469]

47. Fan Y, Sahdev P, Ochyl LJ, Moon JJ. Cationic liposome-hyaluronic acid hybrid nanoparticles for intranasal vaccination with subunit antigens. J Control Release. 2015; 208:121–129. J, J.A. [PubMed: 25869965]

48. Ning N, et al. Cancer stem cell vaccination confers significant antitumor immunity. Cancer Res. 2012; 72:1853–1864. [PubMed: 22473314]

49. Stephan MT, Moon JJ, Um SH, Bershteyn A, Irvine DJ. Therapeutic cell engineering with surface-conjugated synthetic nanoparticles. Nat Med. 2010; 16:1035–1041. [PubMed: 20711198]

50. Anthony DD, Lehmann PV. T-cell epitope mapping using the ELISPOT approach. Methods. 2003; 29:260–269. [PubMed: 12725791]

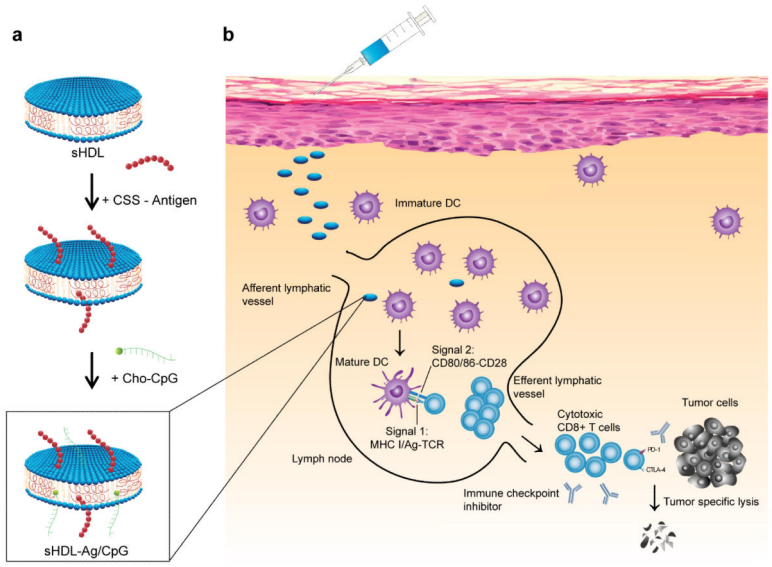

Figure 1. Design of sHDL nanodisc platform for personalized cancer vaccines

a, sHDL nanodiscs, composed of phospholipids and apolipoprotein-1 mimetic peptides (22A), are engineered for co-delivery of antigen (Ag) peptides and adjuvants. Pre-formed sHDL nanodiscs displaying 4 mol% DOPE-PDP are mixed with cysteine-modified Ag peptides, including tumor-specific mutated neo-antigens identified via tumor exome DNA sequencing, and subsequent incubation with cholesterol-modified immunostimulatory molecules (Cho-CpG) leads to formation of sHDL nanodiscs co-loaded with Ag and CpG (sHDL-Ag/CpG). **b,** Upon administration, sHDL nanodiscs efficiently co-deliver Ag and CpG to draining lymph nodes, promote strong and durable Ag presentation by dendritic cells (DCs) (Signal 1), and induce DC maturation (Signal 2), resulting in elicitation of robust Ag-specific CD8α+ cytotoxic T lymphocyte (CTL) responses. Activated CTLs recognize and kill their target cancer cells in peripheral tissues and exert strong anti-tumor efficacy. Combination immunotherapy with immune checkpoint blockade further amplifies the potency of nanodisc vaccination, leading to elimination of established tumors.

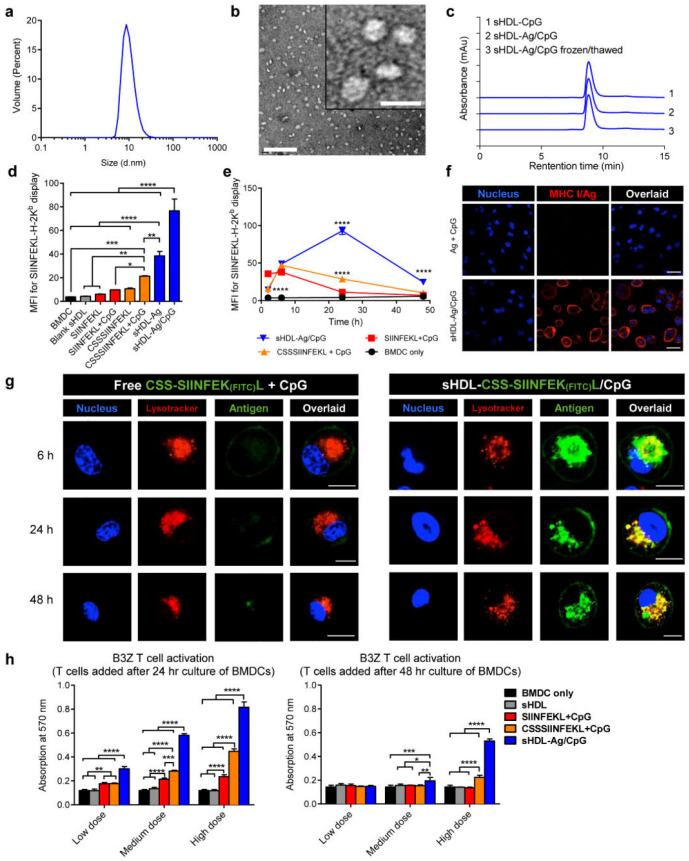

Figure 2. Strong and durable Ag presentation mediated by sHDL nanodiscs

a, Dynamic light scattering analysis and **b,** transmission electron microscopy imaging showed uniform sHDL-Ag/CpG (10.5 nm ± 0.5 average diameter) with nanodisc-like morphology. Scale bar = 100 nm. Scale bar in the inset = 20 nm. **c,** Homogeneity of nanodiscs was maintained after sterile-filtration (0.22 μm), and long-term storage (8 weeks) at −20°C, followed by thawing at 37°C. **d-e,** BMDCs were incubated with vaccine formulations for **d,** 24 h or **e,** indicated lengths of time, and Ag presentation was quantified by flow-cytometry analysis of DCs stained with 25-D1.16 mAb that recognizes SIINFEKL-H-2K^b complex. **f-g,** Confocal microscopy images of JAWSII cells (immature DCs). **f,** JAWSII cells were incubated with free Ag+CpG or sHDL-Ag/CpG for 24 h and stained with 25-D1.16 mAb. Scale bars = 20 μm. **g,** JAWSII cells were incubated with free CSSSIINFEK$_{(FITC)}$L + CpG or sHDL-CSSSIINFEK$_{(FITC)}$L/CpG for 6, 24, or 48 h, followed by staining with Hochest and Lysotracker. Scale bars = 10 μm. **h,** BMDCs were incubated with different concentrations of indicated formulations: low dose = 20 nM SIINFEKL and 3 nM CpG; medium dose = 100 nM SIINFEKL and 15 nM CpG; and high dose = 500 nM SIINFEKL and 75 nM CpG. After incubation for 24 h or 48 h, BMDCs were co-cultured with SIINFEKL-specific B3Z T-cell hybridoma for another 24 h, followed by assessment of T cell activation. The data show mean ± SD from a representative experiment (n = 3) from 2-4 independent experiments. * $p < 0.05$, ** $p < 0.01$, *** $p < 0.001$, and **** $p < 0.0001$, analyzed by (**d**) one-way or (**e,h**) two-way ANOVA with Bonferroni multiple comparisons post-test.

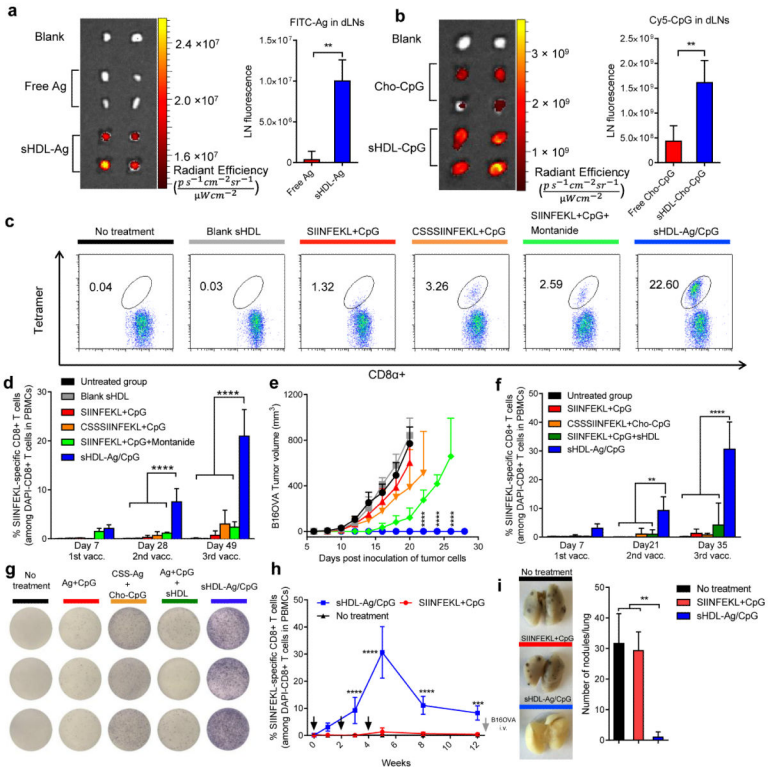

Figure 3. Vaccine nanodiscs for LN-targeting of Ag and adjuvants and elicitation of CTL responses

a-b, C57BL/6 mice were administered subcutaneously at tail base with **a,** 31 nmol FITC-tagged Ag (CSSSIINFEK$_{(FITC)}$L) or **b,** 2.3 nmol Cho-CpG (20% labeled by Cy5) in free soluble or sHDL form, and fluorescence signal in the draining inguinal LNs were quantified with IVIS after 24 h. **c-e,** C57BL/6 mice were immunized with the indicated formulations (15.5 nmol Ag peptide and 2.3 nmol CpG) on days 0, 21, and 42. **c,** Shown are their representative scatter plots on day 49 and **d** the frequency of SIINFEKL-specific CD8α+ T-cells in peripheral blood measured 7 days post each immunization by flow-cytometry analysis of tetramer+ CD8α+ T-cells. **e,** On day 50, pre-vaccinated animals were challenged with subcutaneous flank injection of 2×10^5 B16OVA cells, and tumor growth was measured over time. **f-h,** C57BL/6 mice were immunized in a biweekly interval. Shown are **f,** percent of SIINFEKL-specific CD8α+ T-cells in peripheral blood; **g,** ELISPOT analysis of IFN-γ spot-forming cells among splenocytes after *ex vivo* restimulation with SIINFEKL on day 35; and **h,** Ag-specific CD8α+ T-cell responses measured over 12 weeks post vaccination (black arrows indicate days of immunizations). **i**, Vaccinated mice in **(h)** were intravenously challenged with 5×10^4 B16OVA cells two months after the third vaccination. Shown are pictures of the lungs and numbers of lung metastatic nodules counted on day 20 after the B16OVA challenge. The data show mean ± SD from a representative experiment (n = 4-5) from 2-3 independent experiments. * $p < 0.05$, ** $p < 0.01$, *** $p < 0.001$, and **** $p < 0.0001$, analyzed by (**a-b**) two-tailed unpaired Student's *t* test, (**d,e,f,h**) two-way ANOVA, or (**i**) one-way ANOVA with Bonferroni multiple comparisons post-test. Asterisks in panel **e** indicate statistically significant differences between sHDL-Ag/CpG and SIINFEKL+CpG +Montanide.

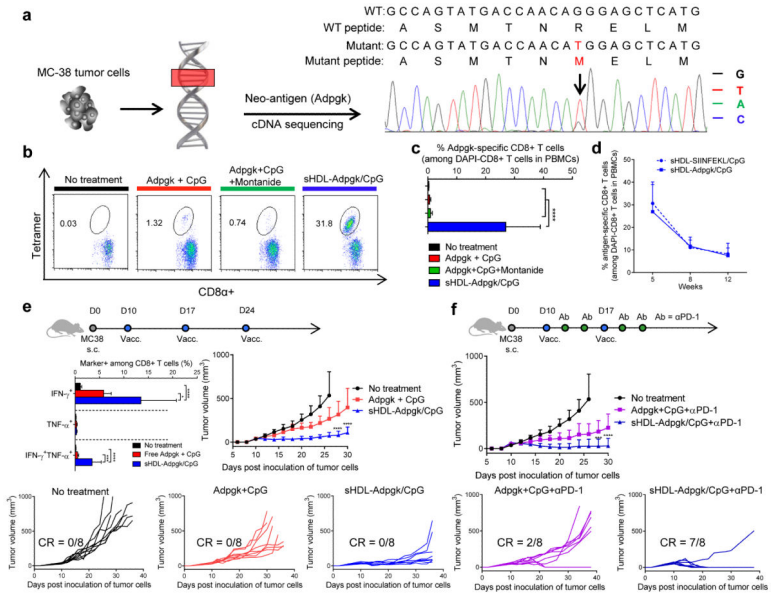

Figure 4. Nanodisc-based neo-antigen vaccination for personalized immunotherapy

a, Mutation of Adpgk in MC-38 murine colon adenocarcinoma cells was confirmed by sequencing cDNA of Adpgk. **b-d,** C57BL/6 mice were vaccinated three times with the indicated formulations (equivalent to 15.5 nmol mutated Adpgk peptide and 2.3 nmol CpG) in a bi-weekly interval, and the frequency of Adpgk-specific CD8α+ T-cells in peripheral blood was measured . Shown are **b**, the representative scatter plots, and **c**, the frequency of Adpgk-specific CTLs on day 35. **d**, Clonal contraction of Ag-specific CD8α+ T-cell responses elicited by sHDL-Adpgk/CpG and sHDL-SIINFEKL/CpG vaccines was monitored for eight weeks after the last vaccination. **e**, C57BL/6 mice were inoculated subcutaneously with 10^5 MC-38 tumor cells and vaccinated with the indicated formulations (equivalent to 15.5 nmol mutated Adpgk peptide and 2.3 nmol CpG) on days 10, 17, and 24. Shown are the percent of intracellular IFN-γ^+, TNF-α^+, and IFN-γ^+TNF-α^+ CD8α+ T-cells in peripheral blood on day 30 after *ex vivo* restimulation with the mutated Adpgk Ag. Average and individual MC-38 tumor growth curves are shown with fraction of complete tumor regression (CR). **f**, C57BL/6 mice were inoculated subcutaneously with 10^5 MC-38 tumor cells and vaccinated with the indicated formulations (equivalent to 15.5 nmol mutated Adpgk peptide and 2.3 nmol CpG) on days 10 and 17. On days 1 and 4 after each vaccination, mice were administered intraperitoneally with αPD-1 (100 μg/mouse). Average and individual MC-38 tumor growth curves are shown. The data show mean ± SD from a representative experiment (n = 5-10) from 2-3 independent experiments. * $p < 0.05$, ** $p < 0.01$, *** $p < 0.001$, and **** $p < 0.0001$, analyzed by (**c**) one-way ANOVA or (**e,f**) two-way ANOVA with Bonferroni multiple comparisons post-test. Asterisks in (**e,f**) indicate statistically significant differences between sHDL-Ag/CpG and all other treatment groups.

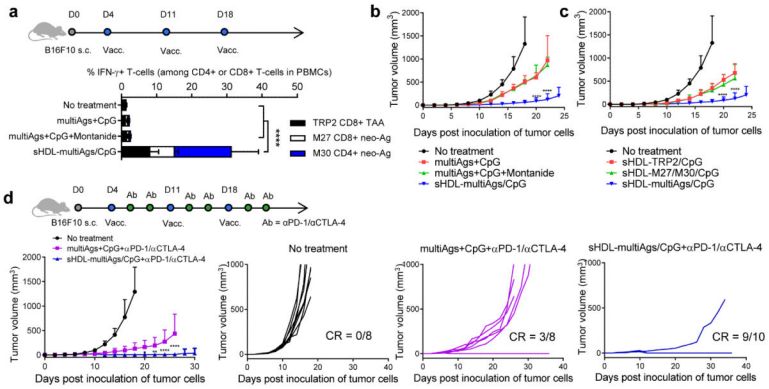

Figure 5. Tumor eradication by combination immunotherapy with multi-epitope vaccine nanodiscs and immune checkpoint blockade

a-d, C57BL/6 mice were inoculated subcutaneously with 10^5 melanoma B16F10 cells and vaccinated on days 4, 11, and 18 with indicated formulations (10 nmol of each antigen peptide and 2.3 nmol of CpG). For the combination immunotherapy, on days 1 and 4 after each vaccination, αPD-1 and αCTLA-4 (100 μg/mouse each) were administered intraperitoneally. Shown are **a**, the percent of IFN-γ^+ CD8α+ or CD4+ T cells in peripheral blood measured by intracellular cytokine staining, and **b-d**, average and individual B16F10 tumor growth curves. The data show mean ± SD from a representative experiment (n = 5-10) from 2-3 independent experiments. * $p < 0.05$, ** $p < 0.01$, *** $p < 0.001$, and **** $p < 0.0001$, analyzed by (**a**) one-way ANOVA or (**b-d**) two-way ANOVA with Bonferroni multiple comparisons post-test. Asterisks in (**b-d**) indicate statistically significant differences between sHDL-Ag/CpG and all other treatment groups.